Check for updates

Journal of Science and Engineering Papers
eISSN- 3094-1182 | pISSN- 3079-8175
DOI- 10.62275/josep.24.1000001

RESEARCH ARTICLE OPEN ACCESS

First-Principles Study of the Structural, Electronic, Optical, Thermodynamic, and Magnetic Properties of Zr-Adsorbed B_n (n= 6-8) Clusters

Mosa Farzana Israt[1] | Md. Rafiqul Islam[1] | Md. Maidul Islam[2] | Md. Kabir Ahamed[1*]

[1]Radiation, Transport and Waste Safety Division, Bangladesh Atomic Energy Regulatory Authority, Dhaka, Bangladesh.
[2]Nuclear Safeguards Division, Bangladesh Atomic Energy Regulatory Authority, Dhaka, Bangladesh.

Correspondence: Md. Kabir Ahamed (fbkabir@gmail.com)

Received: 03 October 2026 | **Revised:** 13 November 2026 | **Accepted:** 15 November 2026 | **Available Online:** 23 November 2026

ABSTRACT

Boron clusters have received significant attention due to their electron-deficient bonding, structural diversity, and potential applications in nanotechnology and advanced functional materials. The structural stability and physical properties of small boron clusters, however, are still not well known when transition metals are adsorbed. The structural, electronic, optical, thermodynamic, and magnetic properties of ZrB_n and Zr_2B_n (n= 6–8) clusters were studied and compared with those of the pristine B_n (n= 6–8) clusters using density functional theory (DFT) at the B3LYP level with the SDD and LanL2DZ basis sets. The structural stability of the clusters was investigated by analyzing adsorption energy, thermodynamic parameters and vibrational frequency analysis. The calculated results show that the Zr-adsorbed bipyramidal structures are more structurally stable than the corresponding pristine and pyramidal clusters. Chemical stability analysis using ionization potential, electron affinity, HOMO–LUMO energy gap, and global reactivity descriptors, however, shows that the bi-pyramidal clusters are, in general, less chemically stable than the pyramidal clusters, except for ZrB_8. The Mulliken population analysis and molecular electrostatic potential (MEP) mapping also revealed notable electronic interactions between zirconium and boron atoms within the clusters, suggesting substantial charge transfer. Further, the magnetic properties of the boron clusters are significantly changed by zirconium adsorption. These findings demonstrate that the adsorption of zirconium has a significant effect on the stability, electronic structure, and magnetic properties of small boron clusters and offer insights into the design of transition-metal-doped boron nanoclusters for use in functional nanomaterials such as nanoelectronics and spintronics.

Keywords: *Boron clusters, Zirconium adsorption, Density functional theory, Structural stability, Electronic properties, Magnetic properties, Optical properties*

1 | Introduction

Over the past few decades, boron clusters have attracted significant attention because of their electron-deficient bonding, multicenter interactions, and remarkable structural and electronic diversity. These exceptional properties of boron nanostructures make them promising candidates for nanoelectronics, superconductivity, catalysis, hydrogen storage, and new materials for the aerospace industry [1-3]. Consequently, the structural and electronic properties of boron clusters have been widely investigated theoretically and experimentally [4–7]. Small boron clusters tend to have planar or quasi-planar structures because of their electron deficiency and aromatic bonding properties [8]. Various isomeric structures have been reported, but the general conclusion is that planar and quasi-planar structures are more stable than the three-dimensional structures for small-sized Bn clusters.

Early theoretical studies established the structural evolution of small boron clusters. Boustani studied B_n (n= 2–14) clusters with ab initio calculations and suggested several energetically favorable planar and quasi-planar geometries [9]. Subsequent photo-

This is an open access article under the terms of the Creative Commons Attribution-ShareAlike 4.0 International license (CC BY-SA 4.0), which permits usage, distribution, and replication in any format as long as the original work is correctly attributed and published here first, and the original work is properly cited.

© 2027 The Author(s). Journal of Science and Engineering Papers

electron spectroscopy and DFT calculations of B_6 and its charged forms showed strong aromatic and antiaromatic features, as well as the vibrational structures of the electronic transitions [10]. Further studies on B_3–B_{15} clusters confirmed that most small boron clusters have planar or quasi-planar structures with significant σ- and π-aromatic stabilization [11–14]. In particular, the neutral B_7 cluster with C_2v symmetry and the regular heptagonal B_8 cluster were found to be the most stable isomers [13,15]. These studies show that the geometric and electronic properties of boron clusters are highly sensitive to cluster size and bonding configuration.

In addition to the pristine boron clusters, transition-metal-doped boron clusters have gained a lot of interest because the adsorption of the transition metal can significantly modify their stability, electronic structure, and magnetic properties [16]. Previous studies on Cr-, Mn-, Fe-, Co-, and Ni-doped boron clusters have shown that partially filled d orbitals introduce strong metal-boron interactions and enhance magnetic behavior [17,18]. Among various transition metals, zirconium is particularly interesting due to its large atomic radius, the presence of several oxidation states, and its high electron-donating power. Moreover, zirconium borides possess remarkable thermal stability, hardness, and superconducting properties, which make Zr-doped boron systems potential materials for advanced functional materials [19]. Zirconium borides show composition-dependent properties: ZrB is a heat insulator and lubricant, ZrB_2 a wear-resistant candidate, and ZrB_{12} a high-temperature-resistant superconducting material. ScB_n (n= 1-12) clusters favor planar or quasiplanar ground states for $n \leq 6$ and nest-like structures for $n \geq 7$, with magic numbers at n = 3, 7, 8, 9, and 11 [20]. The electronic structures of Ag-, Au-, and Cu-doped boron clusters have likewise been studied theoretically [21,22].

Di-metal-doped boron clusters (M_2B_n) have been explored less frequently relative to mono-metal-doped boron clusters [23]. Theoretical studies have been performed on the geometries of Ti_2B_6, Ta_2B_6, V_2B_n, Sc_2B_n, and Ti_2B_n clusters, which showed that the clusters have a strong tendency to form bipyramidal structures with good thermodynamic stability [16, 23–26]. The results of these studies indicate that the incorporation of two transition-metal atoms can greatly enhance the metal–boron bond and modify the electronic and magnetic characteristics of the clusters. However, a systematic investigation of both mono- and di-zirconium-adsorbed B_6–B_8 clusters, including their structural stability, electronic structure, optical response, and magnetic behavior, remains unavailable. Boron nanoclusters and boron-based nanostructures have been synthesized experimentally by various methods, including laser ablation, magnetron sputtering, and chemical vapor deposition (CVD) [26–28].

In this work, density functional theory (DFT) calculations employing the B3LYP functional with the SDD and LanL2DZ basis sets were performed to systematically investigate the structural, electronic, optical, thermodynamic, and magnetic properties of pristine, mono-zirconium-adsorbed (ZrB_n), and di-zirconium-adsorbed (Zr_2B_n) boron clusters (n= 6–8). Special attention was given to the comparison of the pyramidal and bipyramidal adsorption structures to determine the relative structural and chemical stability. The present study presents a detailed picture of the adsorption effects of zirconium on small boron clusters and provides theoretical insights for the design of transition-metal-doped boron nanomaterials that are applicable to the fields of nanoelectronics, optoelectronics, and spintronic devices.

2 | Computational Details

All geometrical optimizations were performed using Density Functional Theory (DFT) as implemented in the Gaussian 16 software package [29]. The exchange-correlation interactions were calculated with the hybrid Becke three-parameter Lee–Yang-Parr (B3LYP) functional [30]. To evaluate the basis-set dependence of the calculated properties, two basis sets, namely Stuttgart/Dresden (SDD) and LanL2DZ [31], were employed throughout the calculations..

The choice of the LanL2DZ basis set was made following the criteria that it gives an effective core potential (ECP) treatment for transition-metal atoms and good computational efficiency for the systems of elements H to Bi [32]. Likewise, the SDD basis set, also developed using effective core potentials and extensively used for transition-metal-based systems, was used to validate and compare the results obtained [33].

The structural, electronic, optical, thermodynamic, and magnetic properties of the pristine B_6, B_7, and B_8 clusters, as well as the mono-adsorbed (ZrB_n) and di-adsorbed (Zr_2B_n) clusters (n= 6-8) were systematically investigated using both basis sets. All calculations were performed under spin unrestricted condition to determine the magnetic properties of the clusters accurately. Time-dependent density functional theory (TD-DFT) with B3LYP/SDD and B3LYP/LanL2DZ was employed subsequently for investigating excited-state and optical properties of the clusters

The adsorption energy $E_{ADS_{Zr_mB_n}}$ was calculated to evaluate the interaction strength between zirconium atoms and the boron clusters according to the following expression [34]:

$$E_{Ads_{Zr_mB_n}} = E_{Zr_mB_n} - \left(E_{B_n} + mE_{Zr}\right) \quad (1)$$

Where m (= 1 or 2) and n (= 6-8) represent the numbers of zirconium and boron atoms, respectively. $E_{ADS_{Zr_mB_n}}$ is the total energy of the optimized Zr_mB_n cluster, while E_{Zr} and E_{B_n} denote the energies of an isolated zirconium atom and the corresponding

pristine boron cluster, respectively.

Thermodynamic parameters such as Gibbs free energy (ΔG), enthalpy (ΔH), and entropy (ΔS) were also calculated to further evaluate the structural stability of the clusters using the following equations [35]:

$$\Delta G = G_{Zr_mB_n} - \left(nG_{Zr} + G_{B_n} \right) \quad (2)$$

$$\Delta H = H_{Zr_mB_n} - \left(nH_{Zr} + H_{B_n} \right) \quad (3)$$

$$\Delta S = \frac{(\Delta H - \Delta G)}{T} \quad (4)$$

where $G_{Zr_mB_n}$ and $H_{Zr_mB_n}$ represent the Gibbs free energy and enthalpy of the optimized Zr_mB_n clusters, respectively, whereas G_{Zr}, H_{Zr}, G_{B_n}, and H_{B_n} correspond to the thermodynamic quantities of the isolated zirconium atom and pristine boron clusters. All thermodynamic properties were evaluated at the standard temperature of 298.15 K.

The electronic properties of the clusters were analyzed through Frontier molecular orbital (FMO) analysis, Mulliken population analysis, molecular electrostatic potential (MEP) mapping and dipole moment calculations. The charge transfer between the zirconium and boron atoms was studied by Mulliken charge analysis, while the MEP maps were used to visualize the charge distribution within the clusters. The dipole moment was calculated to evaluate the charge polarization induced by zirconium adsorption.

To investigate the electronic and chemical stability of the investigated clusters, the energies of the highest occupied molecular orbital (HOMO) and the lowest unoccupied molecular orbital (LUMO) were used to calculate the HOMO–LUMO energy gap (E_g), Fermi level energy (E_{FL}), chemical potential (μ), and Hardness (η). The corresponding quantities were calculated using the following equations:

$$E_g = E_{HOMO} - E_{LUMO} \quad (5)$$

$$E_{FL} = \frac{(E_{HOMO} + E_{LUMO})}{2} \quad (6)$$

where E_{HOMO} is the energy of the highest occupied molecular orbital (HOMO) and E_{LUMO} is the energy the lowest unoccupied molecular orbital (LUMO). Chemical potential (μ) is defined by [36].

$$\mu = -\left(\frac{E_{HOMO} + E_{LUMO}}{2} \right) \quad (7)$$

where (IP) and (EA) are the ionization potential and electron affinity, respectively. Under the Koopmans approximation, these quantities can be estimated from the frontier molecular orbital energies as IP=-E_{HOMO} and EA=-E_{LUMO}. The HOMO represents the frontier orbital with the greatest tendency to donate electron density, whereas the LUMO represents the frontier orbital with the greatest tendency to accept electron density [37].

The chemical hardness η was calculated using the Koopmans approximation [38]:

$$\eta = \frac{IP - EA}{2} \quad (8)$$

where (IP) and (EA) are the ionization potential and electron affinity, respectively [39,40]. The chemical softness (S) and electrophilicity index (ω) were subsequently calculated from the chemical potential and chemical hardness using the following equations [41,36]:

$$S = \frac{1}{2\eta} \quad (9)$$

$$\omega = \frac{\mu^2}{2\eta} \quad (10)$$

Higher chemical hardness and lower softness generally indicate greater resistance to changes in the electronic configuration and, consequently, lower chemical reactivity. The electrophilicity index provides information about the tendency of a system to accept electron density.

Finally, the optical properties of the clusters were explored by using UV-Visible absorption and Circular Dichroism (CD) spectra obtained from TD-DFT calculations. The UV–Visible spectra were analyzed to evaluate the optical absorption properties of the clusters, while the CD spectra were used to assess the optical activity of the clusters. Furthermore, the magnetic moment, spin-density distribution, and electronic density of states (DOS) were calculated to gain insight into the magnetic properties that are induced by the adsorption of zirconium.

In this work, only the B3LYP functional was used, without diffuse functions or a dispersion correction, and spin contamination was not checked. The IP and EA values were estimated from the HOMO and LUMO energies, so the results should be read as trends and not as exact values. Testing with other functionals (e.g., PBE0, TPSSh, M06) is suggested for future work.

3 | Results and discussion

3.1 | Structural Properties

3.1.1 | Equilibrium Geometries

The various properties of pristine and Zr-adsorbed B_n (n = 6-8) clusters were investigated using density functional theory (DFT) with the B3LYP hybrid functional and the SDD and LanL2DZ basis sets. The geometries of the pristine, pyramidal (ZrB_n) and bipyramidal (Zr_2B_n) clusters were optimized, and the resulting structures are shown in Figure 1.

In this study, we have taken hexagonal B_6 ring with D_{2h} symmetry, a B_7 cluster with Cs symmetry obtained by adding one B atom to the B_6 ring, and a zigzag eight-membered B_8 ring with D_4d symmetry, consistent with previous theoretical work [42]. After relaxation, all pristine clusters retain planar geometries, as shown in Figure 1a, 1d and 1g. When Zr atoms are adsorbed on these planar clusters in pyramidal and bipyramidal configurations, all the pyramidal clusters become distorted except ZrB_8 (Figure 1h). In ZrB_6 cluster, three B atoms are out of the B_6 plane, and in case of ZrB_7 cluster, four B atoms are displaced from the plane. The bipyramidal clusters, by contrast, stay planar, with the exception of Zr_2B_6 (Figure 1c), which indicate that bipyramidal structures possess grater stability than pyramidal structures.

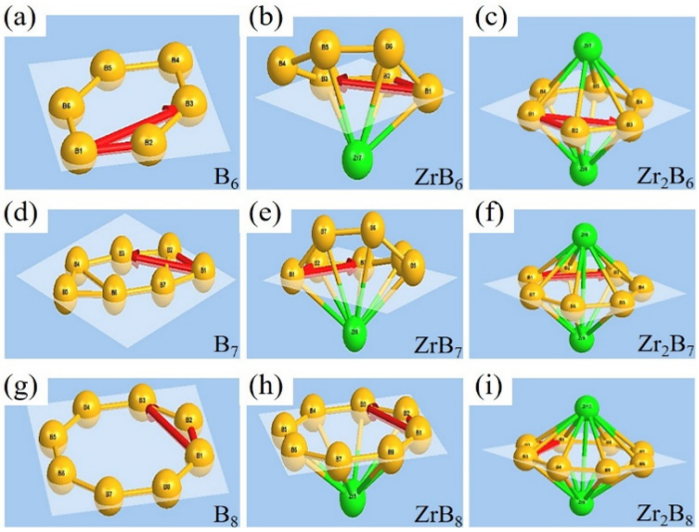

Figure 1 | Equilibrium geometries of optimized (a) B_6, (b) ZrB_6, (c) Zr_2B_6, (d) B_7, (e) ZrB_7, (f) Zr_2B_7, (g) B_8, (h) ZrB_8, and (i) Zr_2B_8 nanoclusters (arrow represents nearest and next nearest in-plane atoms from the origin point).

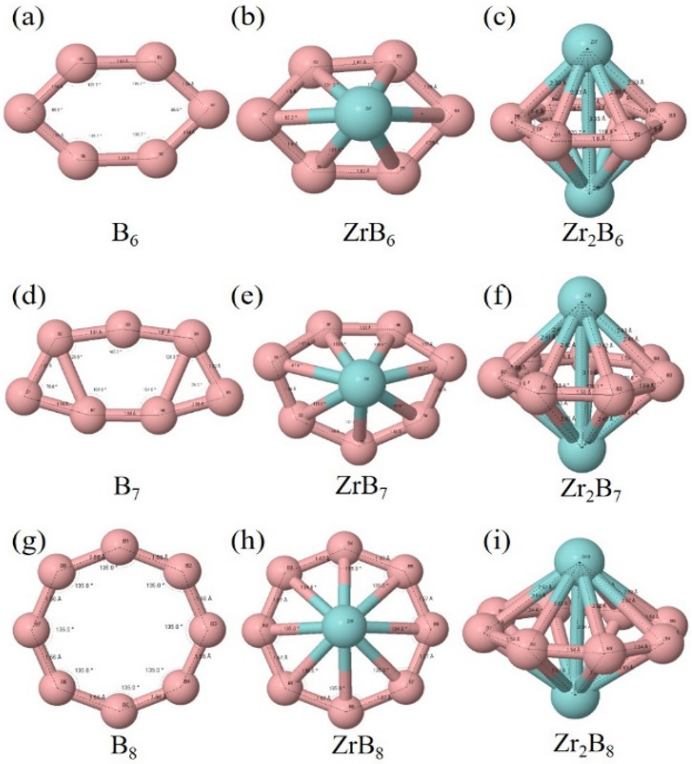

Figure 2 | Schematic illustration of relaxed pristine and adsorbed structures (a) B_6, (b) ZrB_6, (c) Zr_2B_6, (d) B_7, (e) ZrB_7, (f) Zr_2B_7, (g) B_8, (h) ZrB_8, and (i) Zr_2B_8, with bond length and bond angle.

The bond lengths and bond angles between neighboring atoms were also examined before and after Zr adsorption, as shown in Figure 2 and Table 1. The average B-B distance is nearly unchanged by Zr adsorption, remaining between 1.57 and 1.59 Å, which indicates that the boron framework is largely preserved. The Zr-B distance increases slightly with cluster size, from 2.44 to 2.52 Å in the pyramidal clusters and from 2.34 to 2.52 Å in the bipyramidal clusters, so it is longest in the B_8-based clusters. The Zr-Zr distance in the bipyramidal clusters decreases from 3.55 Å in Zr_2B_6 to 3.19 Å in Zr_2B_7 and 3.04 Å in Zr_2B_8. Because the two Zr atoms lie on opposite faces of the B_n ring, this distance depends on the ring size as well as on the Zr-B distance, so the contraction is largely of geometric origin.

3.1.2 | Equilibrium Geometries

Adsorption energy is another key quantity for evaluating the stability of the clusters, since it shows how strongly the Zr atoms are bound to the B_n nanocluster. A more negative adsorption energy indicates stronger binding and a more stable structure. The

Table 1 | Calculated average bond lengths (in Å) for all pristine and Zr-adsorbed B_n clusters using the SDD basis set.

Average bond lengths	Pristine			Pyramidal			Bi-pyramidal		
	B_6	B_7	B_8	ZrB_6	ZrB_7	ZrB_8	Zr_2B_6	Zr_2B_7	Zr_2B_8
B-B	1.57	1.58	1.57	1.59	1.58	1.57	1.59	1.58	1.57
Zr-B	-	-	-	2.44	2.45	2.52	2.34	2.45	2.52
Zr-Zr	-	-	-	-	-	-	3.55	3.19	3.04

Table 2 | Adsorption energies (E_{ads}), Change in enthalpy (ΔH), Gibbs free energy (ΔG) in electron volt unit, Entropy (ΔS) in eVmole^{-1}K^{-1} unit for Zr-adsorbed boron clusters using two basis sets.

System	E_{ads}		ΔG		ΔH		ΔS	
	SDD	*LanL2DZ*	*SDD*	*LanL2DZ*	*SDD*	*LanL2DZ*	*SDD*	*LanL2DZ*
ZrB_6	-7.29	-7.12	-6.94	-6.77	-7.28	-7.11	-0.001	-0.001
Zr_2B_6	-14.91	-14.62	-14.09	-13.79	-14.88	-14.59	-0.003	-0.003
ZrB_7	-7.14	-6.91	-6.66	-6.44	-7.11	-6.87	-0.001	-0.001
Zr_2B_7	-16.31	-15.97	-15.44	-15.09	-16.26	-15.93	-0.003	-0.003
ZrB_8	-9.37	-8.91	-8.87	-8.54	-9.36	-8.91	-0.002	-0.001
Zr_2B_8	-18.76	-18.34	-17.75	-17.36	-18.67	-18.25	-0.003	-0.003

adsorption energies (E_{ads}) of the Zr-adsorbed B_6, B_7 and B_8 clusters are listed in Table 2.

For both basis sets, the adsorption energies become more negative with increasing cluster size. Besides, the adsorption energy of Zr_2B_n clusters is much more negative than that of pyramidal ZrB_n clusters (Figure 3). According to the SDD basis set, the adsorption energies of ZrB_6, ZrB_7, and ZrB_8 are −7.29, −7.14, and −9.37 eV, respectively, while the Zr_2B_6, Zr_2B_7, and Zr_2B_8 clusters have adsorption energies of −14.91, −16.31, and −18.76 eV, respectively. Similar behavior is observed with the LanL2DZ basis set, indicating good agreement between the two computational methods. These results suggest that the adsorption of two zirconium atoms enhances the stability of the boron clusters more effectively than the adsorption of a single zirconium atom. Therefore, the bipyramidal Zr_2B_n clusters are energetically more stable than the corresponding pyramidal ZrB_n clusters.

The thermodynamic parameters, including Gibbs free energy (ΔG), enthalpy (ΔH), and entropy (ΔS), were also calculated to investigate the thermodynamic stability of the investigated clusters. The calculated values are listed in Table 2. The negative values of ΔG indicate that the adsorption process is thermodynamically favorable, whereas the negative values of ΔH confirm that the adsorption process is exothermic. Furthermore, the Zr_2B_n clusters exhibit more negative ΔG and ΔH values than the corresponding ZrB_n clusters, indicating their greater thermodynamic stability (Figure 3).

The calculated entropy changes (ΔS) are also negative for all investigated clusters, suggesting a decrease in randomness during the adsorption process. The larger negative values obtained for the Zr_2B_n clusters indicate that these clusters possess a more ordered structure than the corresponding ZrB_n clusters. Overall, the adsorption energy and thermodynamic analyses consistently demonstrate that the bipyramidal Zr_2B_n clusters are both energetically and thermodynamically more stable than the corresponding pyramidal ZrB_n clusters. The similar trends obtained using the SDD and LanL2DZ basis sets further confirm the reliability of the present calculations.

3.1.3 | Equilibrium Geometries

Vibrational analyses were carried out to investigate the vibrational modes of the pristine and Zr-adsorbed boron clusters. The vibrational spectra were calculated up to 1500 cm^{-1} using the B3LYP/SDD and B3LYP/LanL2DZ levels of theory, and the prominent peak values were also measured. If imaginary frequencies exist in vibrational spectra, it means that the cluster is unstable and has less probability of forming naturally [42].

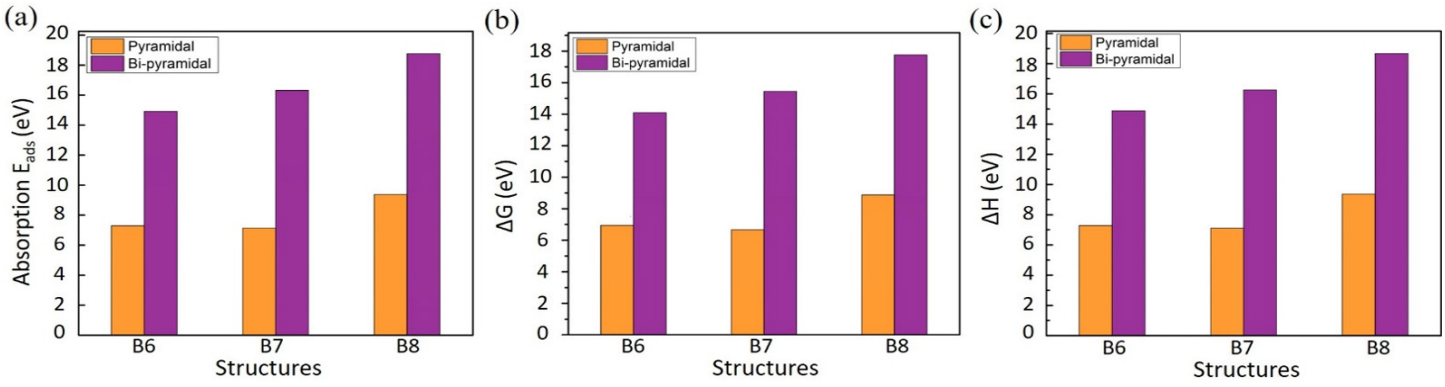

Figure 3 | Illustration of increasing the adsorption energy and thermodynamic parameters (change of Gibbs free energy, enthalpy) from the pyramidal to bipyramidal clusters. Bar diagram of (a) adsorption energy, (b) Gibbs free energy and (c) enthalpy of the pyramidal and bi-pyramidal clusters.

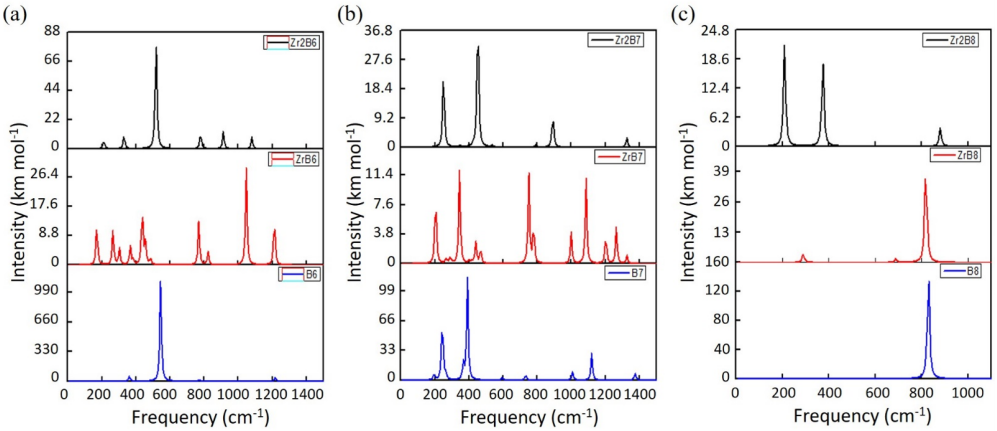

Figure 4 | Infrared ray (IR) spectra analysis for the (a) B_6, (b) B_7 and (c) B_8 System. Blue, red and black colour for pristine, pyramidal and b-ipyramidai structures spectra, respectively.

The B_6 cluster exhibits one imaginary frequency, which indicates that this structure has less probability to exist in nature in a stable form. In contrast, all other investigated clusters exhibit real vibrational frequencies, confirming the stability of their optimized geometries.

The simulated vibrational spectra of all pristine and Zr-adsorbed B_n clusters are presented in Figure 4. For B_6, ZrB_6, and Zr_2B_6, the maximum vibrational intensities of 1193.14, 29.42, and 88.77 km mol^{-1} were observed at vibrational frequencies of 538.42, 1041.53, and 510.53 cm^{-1}, respectively. The first mode is attributed to molecular bending, whereas the latter two are associated with molecular stretching. For B_7, the maximum intensity of 121.15 km mol^{-1} occurs at 383.50 cm^{-1} and is attributed to the bending of the 6B–7B bond. In the ZrB_7 cluster, three high-intensity peaks with intensities of 337.66, 744.47, and 1081.30 km mol^{-1} were observed at vibrational frequencies of 12.41, 11.92, and 11.24 cm^{-1}, respectively, which are attributed to the stretching of 1B–8Zr–5B, 7B–6B, 5B–6B, and 1B–7B bonds. For Zr_2B_7, the maximum vibrational intensity of 49.87 km mol^{-1} occurs at 445.09 cm^{-1} and is attributed to molecular bending. For B_8 and ZrB_8, high-intensity vibrational modes with intensities of 80.67 and 23.57 km mol^{-1} occur at 823.39 and 812.53 cm^{-1}, respectively, and are associated with molecular stretching. For Zr_2B_8, molecular bending and stretching modes exhibit intensities of 11.32 and 19.84 km mol^{-1} at 201.53 and 366.86 cm^{-1}, respectively. These characteristic vibrational modes, particularly those associated with B–Zr interactions, may provide useful information for the experimental identification of the investigated clusters.

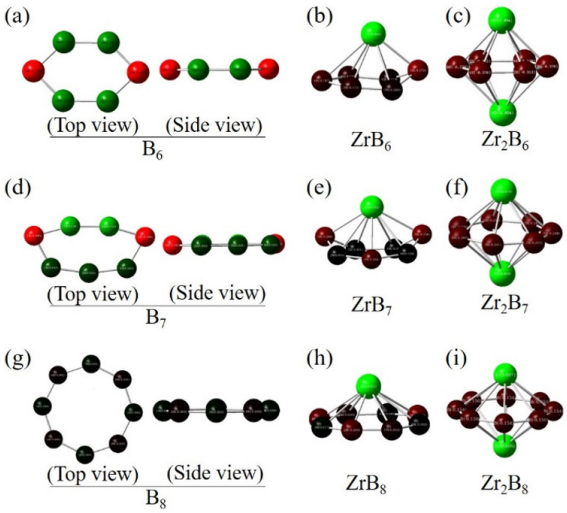

Figure 5 | Optimized structures with Mulliken charge distribution of pristine and Zr adsorbed B_n (n= 6-8) structures in pyramidal and bi-pyramidal configurations. The value of charge distribution increases in the following order Blue>Green>Yellow>Orange>Red> Black.

3.2 | Electronic Properties

3.2.1 | Mulliken Charge Analysis

The Mulliken charge distributions of the clusters were analyzed to investigate the charge transfer between the constituent atoms [43]. The calculated Mulliken charges of pristine and Zr-adsorbed B_n (n= 6–8) obtained using the SDD and LanL2DZ basis sets are presented in Table 3, while the corresponding charge distributions are illustrated in Figure 5. The variation in Mulliken charges for all compounds is also shown in Figure 6. The results show that the Zr atoms generally possess positive Mulliken charges in the Zr-adsorbed clusters, indicating electron-density transfer from Zr to the boron framework.

For the B_6 structure, atoms 1B and 4B accept electron density, whereas the other four atoms (2B, 3B, 5B, and 6B) donate electron density, as shown in Figure 5. For the B_7 structure, atoms 1B and 5B accept electron density, whereas the other five atoms (2B, 3B, 4B, 6B, and 7B) donate electron density. In the case of B_8, the charge distribution among the boron atoms also indicates charge redistribution within the cluster. Upon adsorption of Zr, the charge distribution of the boron framework changes due to the interaction between Zr and B atoms. For the ZrB_6 cluster, the Zr atom exhibits a positive charge, indicating that electron density is transferred from Zr toward the B_6 framework. The

Table 3 | Mulliken Charge distribution for Zr atom 'q' (e) and total system 'Q' (e), Dipole moment 'DM' (Debye), ionization potentials (IP) in eV and electron affinities (EA) in eV in the pristine and Zr adsorbed B_n systems.

Property	Basis set	B_6	ZrB_6	Zr_2B_6	B_7	ZrB_7	Zr_2B_7	B_8	ZrB_8	Zr_2B_8
q	SDD	-	0.89	1.05	-	0.95	0.87	-	0.93	0.72
	LanL2DZ	-	0.63	0.59	-	0.65	0.59	-	0.65	0.61
Q	SDD	0.29	0.89	1.05	0.19	0.95	0.87	0.001	0.93	0.72
	LanL2DZ	0.29	0.66	0.59	0.19	0.65	0.59	0.001	0.65	0.61
DM	SDD	0	7.56	0.0007	0.17	6.53	0.004	0	5.26	0.013
	LanL2DZ	0	7.51	0.0002	0.17	6.39	0.004	0	5.14	0.001
IP	SDD	5.61	5.42	4.64	6.63	5.70	4.85	5.90	6.18	5.04
	LanL2DZ	5.61	5.42	4.76	6.63	5.79	4.95	5.90	6.17	5.11
EA	SDD	4.83	3.41	3.16	4.62	3.21	3.43	4.73	4.77	2.85
	LanL2DZ	4.84	3.36	3.27	4.62	3.18	2.33	4.74	4.74	2.84

boron atoms directly involved in the interaction with Zr show corresponding changes in their Mulliken charges. A similar charge-transfer behavior is observed for ZrB_7 and ZrB_8, where the Zr atom carries a positive charge and the boron framework acquires electron density. The charge redistribution is more pronounced around the B atoms interacting directly with the Zr atom.

For the bipyramidal Zr_2B_6, Zr_2B_7, and Zr_2B_8 clusters, both Zr atoms exhibit positive Mulliken charges, indicating electron-density transfer from the two Zr atoms toward the corresponding boron frameworks. The charge distribution over the boron atoms changes with the cluster size, while the two Zr atoms remain electron deficient relative to the B atoms. The charge-transfer behavior observed in the Zr_2B_n clusters are is therefore consistent with the interaction between the electropositive Zr atoms and the electron-deficient boron framework.

The observed charge redistribution can be qualitatively explained by the difference in Pauling electronegativity between B (2.04) and Zr (1.33). Since Zr is less electronegative than B, electron density tends to be transferred from Zr toward the boron framework upon cluster formation. Overall, the Mulliken charge analysis confirms the occurrence of charge redistribution between Zr and B atoms in the investigated clusters and provides evidence for the interaction between the Zr atoms and the boron framework.

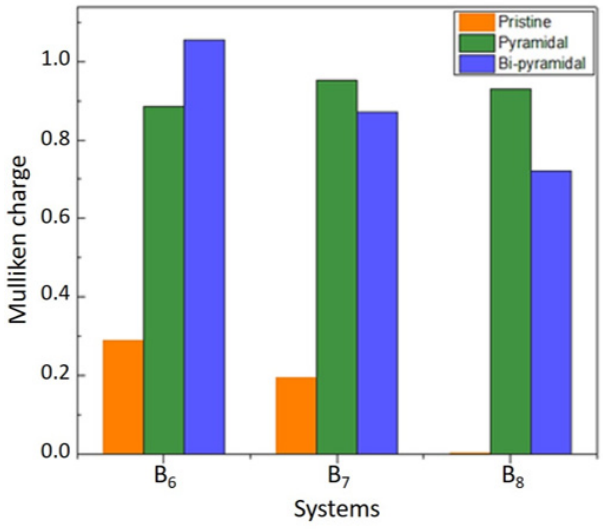

Figure 6 | Variation of Mulliken charge for pristine and Zr-adsorbed B_n clusters.

3.2.2 | Molecular Electrostatic Potential Mapping

The molecular electrostatic potential (MEP) surface was calculated to investigate the distribution of positive and negative electrostatic potential over the surfaces of the pristine and Zr-adsorbed B_n (n= 6–8) clusters. MEP analysis provides useful information regarding the charge distribution and the electron-rich and electron-deficient regions of the investigated clusters [44,45]. The calculated MEP maps around the adsorption sites are presented in Figure 7. The color scale represents the electrostatic potential, with red and blue corresponding to the negative and positive extremes, respectively [46].

The MEP maps show that, for all Zr-adsorbed B_n clusters, a positive electrostatic potential (blue region) is mainly localized around the Zr atom, whereas a negative electrostatic potential (red region) is predominantly distributed over the B_n framework. The negative potential region represents an electron-rich region, while the positive potential region corresponds to an electron-deficient region. The observed separation of positive and negative electrostatic potential indicates charge redistribution between the Zr atoms and the boron framework upon adsorption. The MEP distributions of both the pyramidal and bipyramidal clusters are consistent with the charge-transfer behavior obtained from the Mulliken population analysis. These results indicate that the Zr atoms act as electron-deficient centers, whereas the boron framework provides relatively electron-rich regions in the

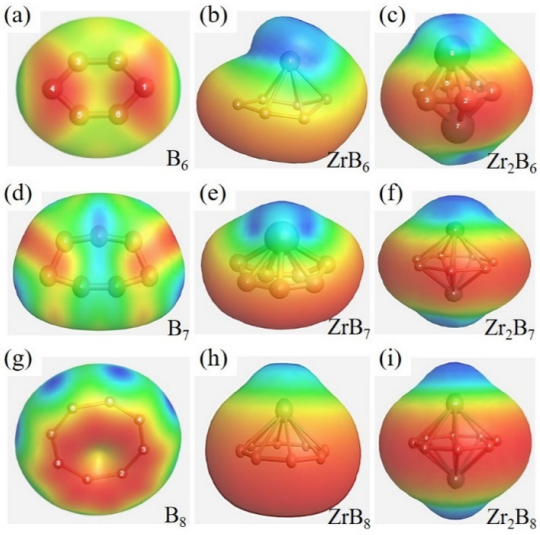

Figure 7 | Variation of Mulliken charge for pristine and Zr-adsorbed B_n clusters.

investigated Zr-adsorbed clusters.

3.2.3 | Ionization Potential (IP), Electron Affinity (EA) and Dipole Moment (μD)

The ionization potential (IP), electron affinity (EA) and dipole moment provide predictions of the electronic properties of the nanoclusters. The ionization potential is defined as the energy required to remove an electron from a molecule. Among the different types of IP, including the Koopmans, vertical, and adiabatic IP, here we investigated Koopmans approximation, so these values are approximate and are used only to compare trends among the clusters. Also, electron affinity (EA) is defined as the energy released when an electron is added to a system. It is related to the energy of the E_{HOMO} and E_{LUMO}. A higher IP means a greater resistance to losing an electron, and a lower EA means a lower tendency to accept an electron[47]. The IP and EA values of our studied structures are listed in Table 3, while the variations with cluster size are presented in Figure 8. The pristine B_n clusters usually have higher IP and EA values than the Zr-adsorbed clusters. The exception is ZrB_8, which has a higher IP than B_8 and almost the same EA. The lower EA of the Zr-adsorbed clusters means they accept extra electrons less easily. The bipyramidal Zr_2B_n clusters have the lowest IP and EA values. This means they lose electrons more easily and accept electrons less easily than the pyramidal and pristine clusters. Thus, adsorbing the Zr atoms significantly alters the electronic properties of the nanoclusters.

The dipole moment of a cluster provides information about the asymmetry of its charge distribution [48]. A nonzero dipole moment arises from an asymmetric distribution of charge within the cluster. The calculated dipole moments (μD) of the pristine and Zr-adsorbed B_n clusters are presented in Table 3. The B_6 and B_8 clusters exhibit nearly zero dipole moments, indicating their highly symmetric charge distributions, whereas B_7 possesses a dipole moment of 0.174 Debye. For the pyramidal ZrB_n clusters, the charge distributions are asymmetric, resulting in relatively large dipole moments of 7.560, 6.531, and 5.264 Debye for ZrB_6, ZrB_7, and ZrB_8, respectively. In contrast, the dipole moments of the bipyramidal Zr_2B_n (n = 6–8) clusters are nearly zero, indicating relatively symmetric charge distributions. These results are consistent with the more symmetric charge distribution of the bipyramidal structures and support their comparatively lower chemical reactivity.

3.2.4 | Chemical Potential and Global Indices

To further investigate the electronic stability and chemical reactivity of the pristine and Zr-adsorbed B_n (n = 6–8) clusters, the chemical potential (μ), chemical hardness (η), softness (S), and electrophilicity index (ω) were calculated using the SDD and LanL2DZ basis sets. The calculated values are presented in Table 4. The chemical potential values are negative for all investigated clusters. For the SDD basis set, the chemical potential values are −5.22, −4.42, and −3.90 eV for B_6, ZrB_6, and Zr_2B_6, respectively. Similarly, the corresponding values for B_7, ZrB_7, and Zr_2B_7 are −5.63, −4.46, and −3.64 eV, respectively, while those for B_8, ZrB_8, and Zr_2B_8 are −5.31, −5.48, and −3.95 eV, respectively. The varia-

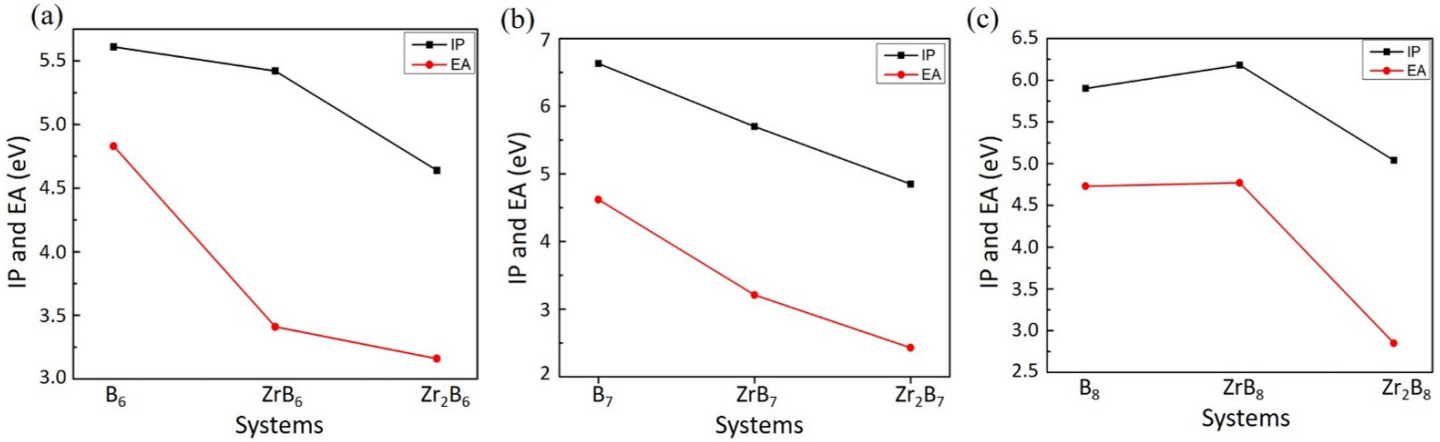

Figure 8 | The variation of Ionization Potential (IP) and Electron Affinity (EA) of pristine and Zr adsorbed (a) B_6, (b) B_7 and (c) B_8 nanoclusters.

Table 4 | Chemical potential (μ) in eV, hardness (η) in eV, softness (S) in eV^{-1}, electrophilicity (ω) in eV for boron clusters.

Property	Basis set	B_6	ZrB_6	Zr_2B_6	B_7	ZrB_7	Zr_2B_7	B_8	ZrB_8	Zr_2B_8
μ	SDD	-5.22	-4.42	-3.90	-5.63	-4.46	-3.64	-5.31	-5.48	-3.95
	LanL2DZ	-5.23	-4.39	-4.01	-5.63	-4.48	-3.64	-5.31	-5.45	-3.98
η	SDD	0.39	1.01	0.74	1.01	1.25	1.21	0.59	0.71	1.09
	LanL2DZ	0.39	1.03	0.75	1.01	1.31	1.31	0.58	0.71	1.14
S	SDD	1.28	0.50	0.68	0.50	0.40	0.41	0.86	0.71	0.46
	LanL2DZ	1.29	0.49	0.67	0.50	0.38	0.38	0.86	0.70	0.44
ω	SDD	34.93	9.70	10.28	15.74	7.97	5.46	24.15	21.26	7.11
	LanL2DZ	35.16	9.35	10.79	15.75	7.69	5.05	24.23	20.83	6.96

tion in chemical potential following Zr adsorption indicates that the electronic properties of the boron clusters are substantially modified by interaction with Zr atoms.

Chemical hardness is an important global reactivity descriptor that provides information about the resistance of a system to changes in its electronic configuration [49]. Higher chemical hardness is generally associated with lower chemical softness and reduced chemical reactivity. As shown in Figure 9, the chemical hardness of the Zr-adsorbed clusters is generally higher than that of the corresponding pristine B_n clusters. For example, using the SDD basis set, the hardness values of B_6, ZrB_6, and Zr_2B_6 are 0.39, 1.01, and 0.74 eV, respectively, whereas those of B_7, ZrB_7, and Zr_2B_7 are 1.01, 1.25, and 1.21 eV, respectively. For B_8, ZrB_8, and Zr_2B_8, the corresponding hardness values are 0.59, 0.71, and 1.10 eV, respectively. The increase in chemical hardness upon Zr adsorption suggests that the Zr-containing clusters are chemically harder and less susceptible to changes in their electronic configuration than the corresponding pristine clusters.

The calculated softness values exhibit an inverse relationship with chemical hardness. The pristine B_n clusters generally show higher softness values than the corresponding Zr-adsorbed clusters, indicating a greater tendency toward electronic reorganization and chemical interaction. In contrast, the lower softness values of the Zr-containing clusters are consistent with their higher chemical hardness. Among the investigated systems, the bipyramidal Zr_2B_n clusters generally exhibit relatively high hardness and low softness, suggesting comparatively lower chemical reactivity within the framework of the global reactivity descriptors.

The electrophilicity index (ω) provides an additional measure of the tendency of a system to accept electron density. The calculated electrophilicity values generally decrease following Zr adsorption, particularly for the bipyramidal Zr_2B_n clusters as presented in Figure 9. For the SDD basis set, the electrophilicity values are 34.93, 9.70, and 10.28 eV for B_6, ZrB_6, and Zr_2B_6, respectively. For B_7, ZrB_7, and Zr_2B_7, the corresponding values are 15.74, 7.97, and 5.46 eV, while for B_8, ZrB_8, and Zr_2B_8 they are 24.15, 21.26, and 7.11 eV, respectively. The lower electrophilicity values of the Zr-containing clusters indicate a reduced tendency to accept additional electron density compared with the corresponding pristine clusters. Overall, the combined increase in chemical hardness and decrease in softness and electrophilicity indicate that Zr adsorption substantially modifies the chemical reactivity of the boron clusters and generally produces chemically harder and less reactive systems.

3.2.5 | HOMO-LUMO analysis

The highest occupied molecular orbital (HOMO) and lowest unoccupied molecular orbital (LUMO) are important frontier mo-

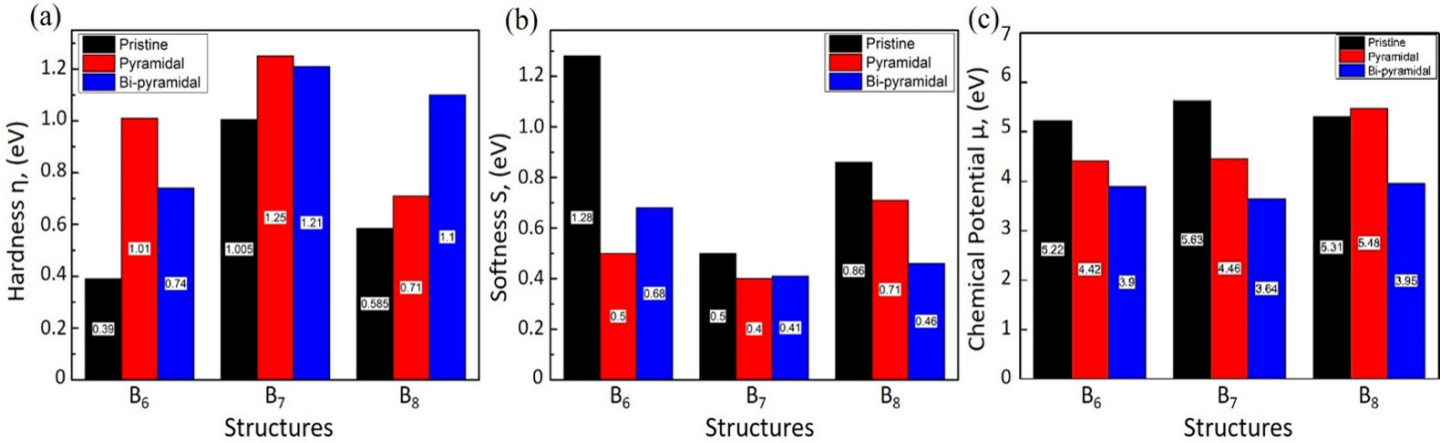

Figure 9 | The size dependence variation of (a) hardness, (b) softness and (c) chemical potential for all B_n and Zr-adsorbed B_n clusters.

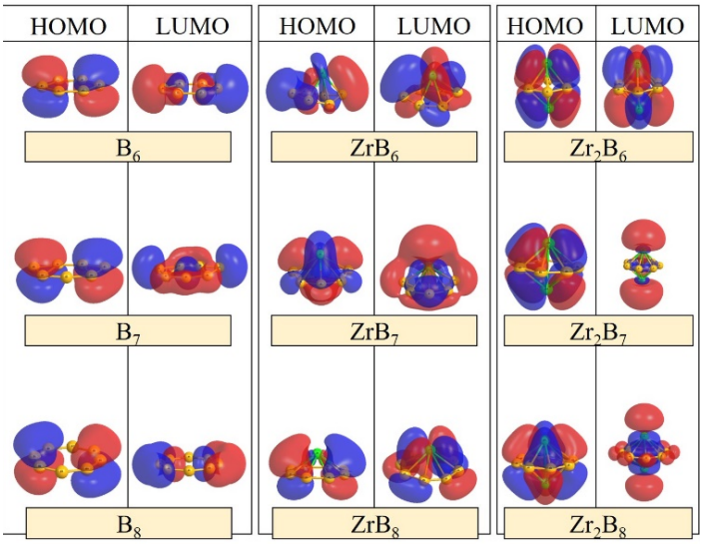

Figure 10 | The contour maps of the HOMO and LUMO for pristine and Zr-adsorbed B_n cluster.

lecular orbital descriptors for understanding the electronic structure and chemical reactivity of molecular clusters [50]. The spatial distributions of the frontier orbitals can also provide information about the regions involved in electron donation and electron acceptance [51]. In the present study, the HOMO and LUMO energies were calculated using both the DFT/SDD and DFT/LanL2DZ levels of theory. The HOMO, HOMO−10, LUMO, and LUMO+10 energies were also examined to evaluate the orbital-energy-level behavior of the investigated clusters, and the corresponding values are provided in the Supplementary Information. The electronic properties of the pristine and Zr-adsorbed B_n clusters were further analyzed in terms of the HOMO–LUMO energy gap (E_g), which is widely used as a qualitative descriptor of chemical stability and reactivity.

The HOMO and LUMO contour maps of the pristine and Zr-adsorbed B_n clusters are presented in Figure 10. The HOMO–LUMO gaps calculated using the SDD basis set are also compared in Figure 10 and Table 5. Upon adsorption of Zr on the B_n clusters in both pyramidal and bipyramidal configurations, the HOMO–LUMO gap generally increases.

A comparison between the pyramidal and bipyramidal Zr-adsorbed clusters shows that the bipyramidal structures possess smaller (E_g) values than the corresponding pyramidal structures for ZrB_6 and ZrB_7. In contrast, for the Zr-adsorbed B_8 system, the bipyramidal structure exhibits a higher (E_g) value than the corresponding pyramidal structure. Interestingly, the pyramidal Zr-adsorbed B_n clusters exhibit the largest HOMO–LUMO gaps among the investigated clusters, except for ZrB_8. The relatively larger (E_g) values suggest comparatively lower chemical reactivity and greater resistance to electronic excitation within the framework of the frontier-orbital analysis. In contrast, clusters with smaller HOMO–LUMO gaps are expected to exhibit relatively higher chemical reactivity. These results are consistent with the trends obtained from the global reactivity descriptors, particularly chemical hardness and softness, and demonstrate that Zr adsorption significantly modifies the electronic properties of the boron clusters.

3.2.6 | Density of states (DOS)

To further elucidate the electronic structure of the investigated clusters, the density of states (DOS) was analyzed. The DOS describes the distribution and availability of electronic states as a function of energy and provides useful information about the electronic structure and frontier-state characteristics of a cluster [52]. The calculated total density of states (TDOS) spectra of the pristine and Zr-adsorbed B_n (n= 6–8) clusters are presented in Figure 11. The energy region with negligible or zero DOS corresponds to an absence of available electronic states and is associated with the HOMO–LUMO gap of the cluster. The DOS profiles also illustrate the redistribution of electronic states resulting from the interaction between the Zr atoms and the boron framework.

The DOS spectra show that the electronic-state distributions of the Zr-adsorbed clusters differ from those of the corresponding pristine B_n clusters. In particular, the separation between the oc-

Table 5 | HOMO-LUMO energies (E_{HOMO} and E_{LUMO}) in eV, Fermi level energy (E_{FL}) in eV, HOMO-LUMO gap (E_g) in eV for boron clusters.

Property	Basis set	B_6	ZrB_6	Zr_2B_6	B_7	ZrB_7	Zr_2B_7	B_8	ZrB_8	Zr_2B_8
E_{Homo}	SDD	-5.61	-5.42	-4.64	-6.63	-5.70	-4.85	-5.90	-6.18	-5.04
	LanL2DZ	-5.61	-5.42	-4.76	-6.63	-5.79	-4.94	-5.90	-6.17	-5.11
E_{Lumo}	SDD	-4.83	-3.41	-3.16	-4.62	-3.21	-2.43	-4.73	-4.77	-2.85
	LanL2DZ	-4.83	-3.36	-3.27	-4.62	-3.18	-2.33	-4.74	-4.74	-2.84
E_g	SDD	0.78	2.01	1.48	2.01	2.49	2.42	1.17	1.41	2.19
	LanL2DZ	0.78	2.06	1.49	2.01	2.62	2.62	1.17	1.43	2.27
E_{FL}	SDD	-5.22	-4.41	-3.90	-5.63	-4.46	-3.64	-5.31	-5.48	-3.95
	LanL2DZ	-5.23	-4.39	-4.01	-5.63	-4.48	-3.64	-5.32	-5.45	-3.98

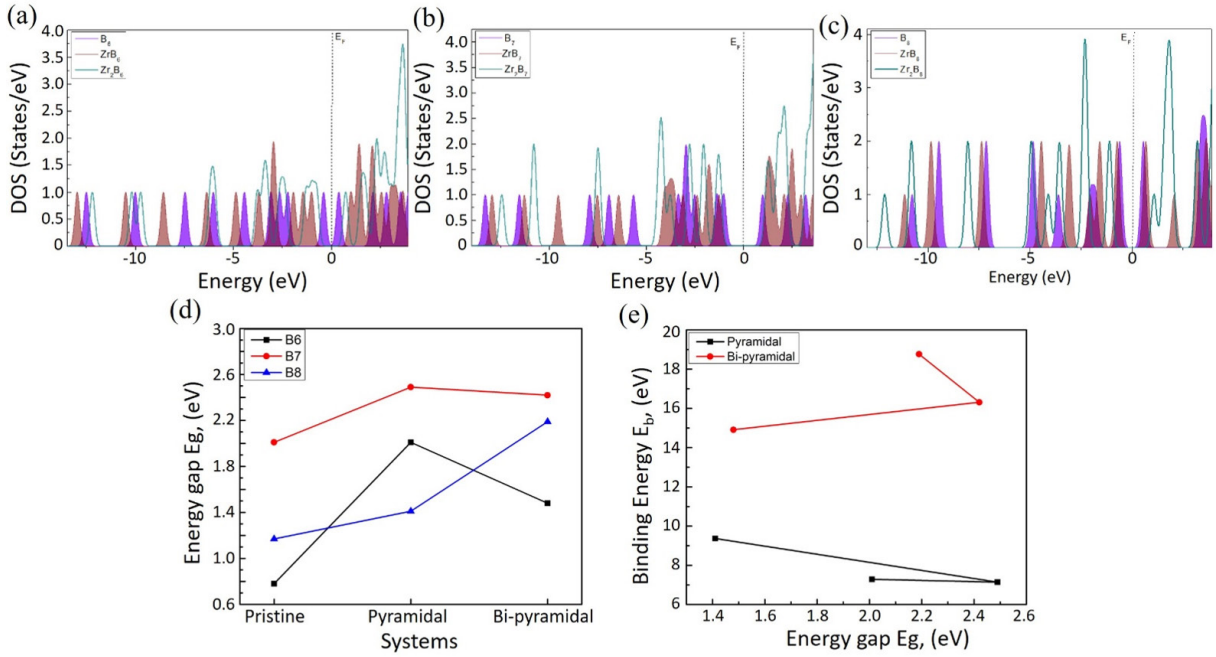

Figure 11 | Density of states (DOS) spectra of pristine and (a) Zr-adsorbed B_6, (b) Zr-adsorbed B_7, (c) Zr-adsorbed B_8 clusters. (d) Comparison of the energy gap among the pristine and Zr-adsorbed B_6, B_7, and B_8 clusters and (e) illustration of the variation of adsorption energy with the energy gap.

cupied and unoccupied frontier states generally increases upon Zr adsorption, consistent with the HOMO–LUMO gap analysis discussed in the previous section. The increase in the frontier-state separation indicates a reduced availability of electronic states near the frontier region and suggests a comparatively lower electronic reactivity of the Zr-adsorbed clusters. These results are consistent with the increase in chemical hardness observed for the Zr-containing clusters. Overall, the DOS analysis supports the conclusion that Zr adsorption significantly modifies the electronic structure of the pristine boron clusters.

3.3 | Magnetic Properties

The magnetic moment is obtained from the difference between the numbers of spin-up and spin-down electrons, and the spin density is the difference between the spin-up and spin-down electron densities. The spin multiplicities of the pristine and Zr-adsorbed B_n (n = 6-8) clusters were set by the number of electrons. The B_6- and B_8-based clusters have an even number of electrons and were calculated as singlets, which have zero total magnetic moment. The B_7-based clusters (B_7, ZrB_7 and Zr_2B_7) have an odd number of electrons, so they must have at least one unpaired electron, and they were calculated as doublets.

To further investigate the origin and spatial distribution of the magnetic moments, spin-density analysis was performed for the odd-numbered clusters. Figure 12 presents the difference between the spin-up and spin-down electron densities for B_7, ZrB_7, and Zr_2B_7. The spin density of ZrB_7 and Zr_2B_7 is predominantly localized around the Zr sites, indicating a major contribution from the Zr atoms to the total magnetic moment. In Zr_2B_7, however, the spin density also extends over the boron framework, indicating that both Zr and B atoms contribute to the overall magnetic behavior. The observed spin-density distributions are consistent with the calculated total magnetic moments of the investigated clusters.

To further elucidate the origin of the magnetic behavior, the total density of states (TDOS) was analyzed for B_7, ZrB_7, and Zr_2B_7. The spin-resolved DOS spectra are presented in Figure 13, where the positive and negative DOS values represent the spin-up and spin-down channels, respectively, and the vertical dashed line indicates the Fermi level. A pronounced difference between the

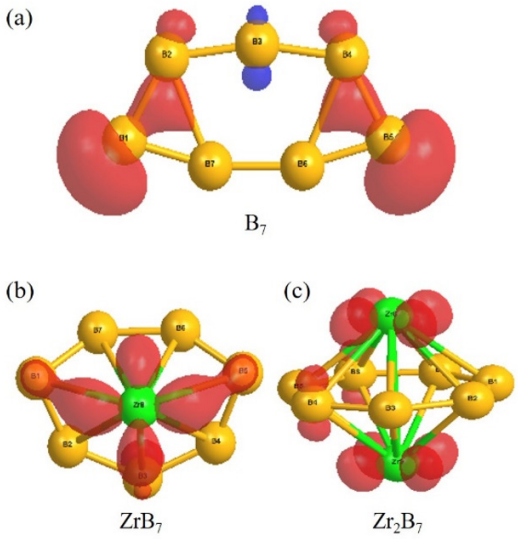

Figure 12 | The difference between the charge density for up-spin and down-spin electrons of the B_7, ZrB_7, and Zr_2B_7 clusters.

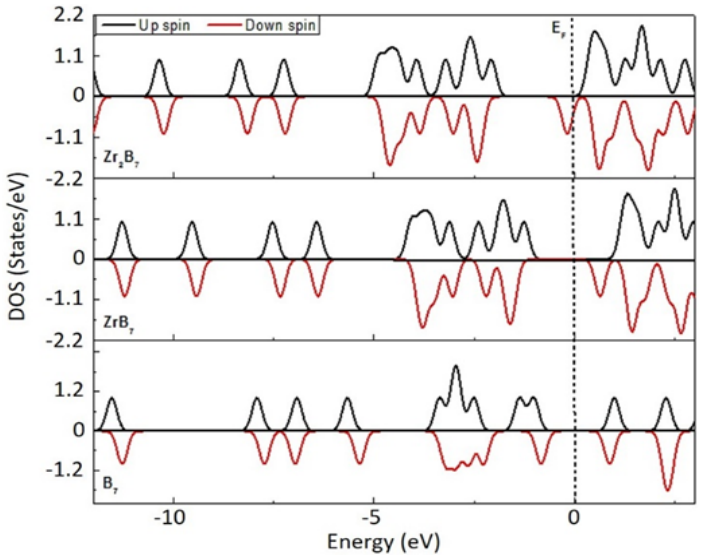

Figure 13 | Computed total density of states of B_7 and Zr-adsorbed B_7 systems for spin-up and spin-down. The vertical dash line denotes the Fermi level. DOS for the majority and minority spin channels are illustrated by the +eV and −eV values, respectively.

spin-up and spin-down DOS distributions is observed upon Zr adsorption, particularly for ZrB_7 and Zr_2B_7, indicating substantial spin polarization near the Fermi level. The spin-dependent electronic states become increasingly asymmetric from the pristine B_7 cluster to the Zr-containing clusters, which is consistent with the enhancement of the total magnetic moment. In particular, Zr_2B_7 exhibits a pronounced spin-dependent electronic structure, with a finite DOS near the Fermi level in one spin channel and a suppressed DOS in the opposite spin channel. This behaviour indicates a strong spin-polarized character and is consistent with the spin-resolved DOS analysis [53].

3.4 | Optical Properties

Optical property of a substance determines the behavior of the substance's interaction with the electromagnetic radiation. From the optical properties, we have investigated absorption spectra in the range of absorbed wavelengths of light and the optical activity of our clusters for potential applications by investigating CD spectra.

3.4.1 | Absorption Spectra Analysis

The optical absorption spectra of the pristine and Zr-adsorbed B_n (n= 6-8) clusters were investigated to examine their responses to electromagnetic radiation in the ultraviolet–visible region. The spectra are presented in Figure 14, and both the absorption intensity and the peak position change upon Zr adsorption [54].

For the pristine B_6 cluster, the main absorption occurs in the wavelength range of approximately 450–600 nm. Upon Zr adsorption, the absorption intensity decreases, indicating a hypochromic effect, while the corresponding absorption peak shifts toward shorter wavelengths, indicating a hypsochromic or blue shift. The bipyramidal Zr_2B_6 cluster also exhibits a hypochromic effect compared with the other investigated B_6 clusters. In Figure 14a, the main band of pristine B_6 at about 525 nm (intensity of about 8600) is largely suppressed in ZrB_6, whose strongest bands appear at about 325 and 410 nm (intensities of about 6400 and 3900), while Zr_2B_6 shows a broad band between 450 and 620 nm (intensity of about 4000). In the case of B_7, Zr adsorption produces a hypsochromic shift accompanied by an increase in absorption intensity, indicating a hyperchromic effect. A similar hyperchromic behavior is observed for Zr_2B_7, which exhibits relatively high absorption intensity compared with the corresponding pristine and pyramidal systems. In Figure 14b, the strongest band of B_7 lies at about 480 nm (intensity of about 3100), compared with about 325 nm (about 6400) for ZrB_7 and about 500 nm (about 5800) for Zr_2B_7, and the broad near-infrared band of B_7 near 950 nm is absent in Zr_2B_7. For the B_8-based clusters, the pristine B_8 cluster exhibits higher absorption intensity than ZrB_8 and Zr_2B_8. In addition, the absorption peaks of ZrB_8 shift toward longer wavelengths, indicating a bathochromic or red shift. In Figure 14c, the single band of B_8 at about 655 nm (intensity of

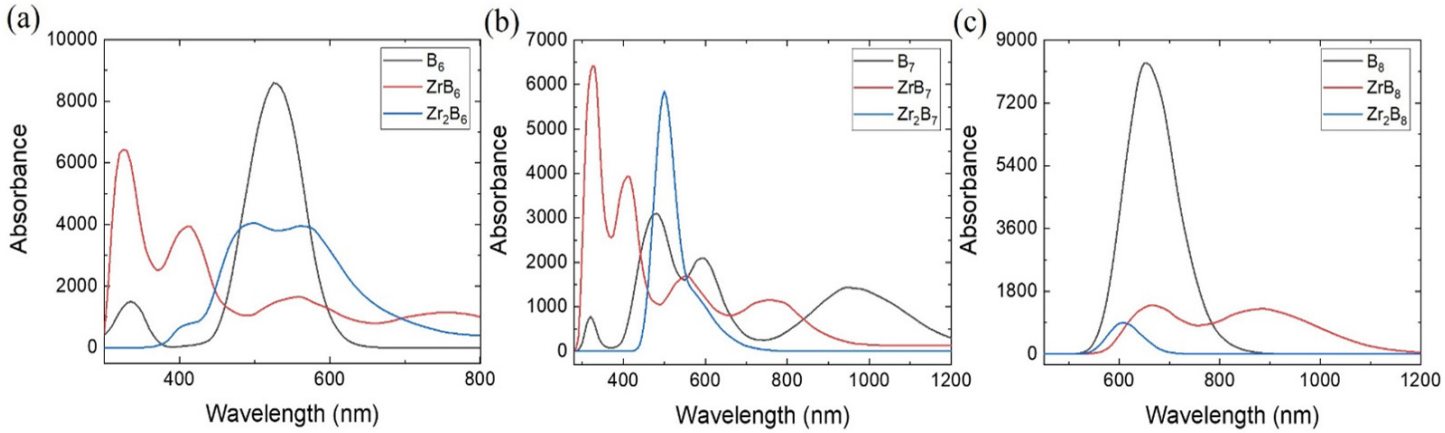

Figure 14 | Absorption spectra of a) pristine and Zr-adsorbed B_6, b) pristine and Zr-adsorbed B_7 and c) pristine and Zr-adsorbed B_8 clusters. Absorbance is a dimensionless quantity and has no unit.

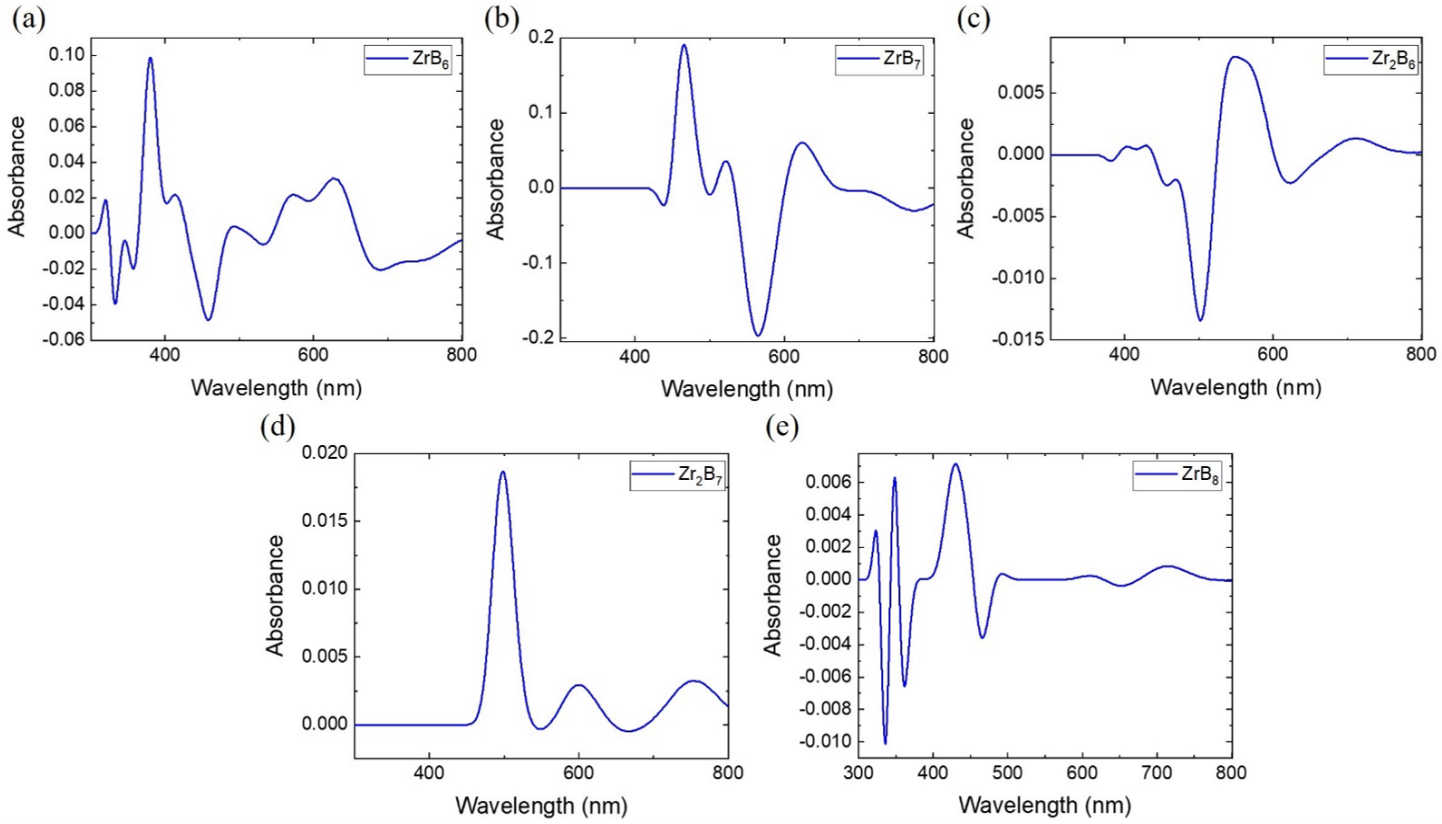

Figure 15 | CD spectra of Zr-adsorbed B_n (n= 6-8) clusters. Absorbance is a dimensionless quantity and has no unit.

about 8300) decreases to about 1400 for ZrB_8, which also shows a weaker band near 890 nm, and to about 900 for Zr_2B_8.

Overall, the calculated spectra demonstrate that Zr adsorption substantially modifies both the intensity and spectral position of the absorption bands of the boron clusters. The observed blue shifts correspond to transitions occurring at relatively higher excitation energies, whereas the red shift observed for ZrB_8 indicates a transition toward lower excitation energy. Among the investigated clusters, the pyramidal structures generally exhibit absorption at shorter wavelengths than the corresponding bipyramidal structures, except for ZrB_8. These distinct absorption characteristics suggest that the investigated Zr-adsorbed boron clusters may be of interest for further studies of optoelectronic and other light-responsive applications.

3.4.2 | Circular Dichroism (CD) spectra analysis

Circular dichroism (CD) refers to the differential absorption of left- and right-circularly polarized light by a chiral system and provides useful information about the chiroptical properties of molecular structures [55,56]. In the present study, the CD spectra of the investigated pristine and Zr-adsorbed B_n (n= 6–8) clusters were calculated using both the SDD and LanL2DZ basis sets. The two basis sets produce qualitatively similar CD spectral features; therefore, the results obtained using the SDD basis set are presented in Figure 15 for clarity.

The calculated CD spectra reveal distinct chiroptical responses for the Zr-adsorbed clusters. The pyramidal ZrB_n (n= 6–8) clusters and the bipyramidal Zr_2B_6 and Zr_2B_7 clusters exhibit nonzero CD signals, indicating the presence of chiroptical responses in these structures. In contrast, the pristine B_n (n= 6–8) clusters and the bipyramidal Zr_2B_8 cluster show negligible or no CD response within the calculated spectral range. These results indicate that Zr adsorption can significantly modify the chiroptical properties of the boron clusters. The nonzero CD responses of ZrB_n (n= 6–8) and Zr_2B_n (n= 6, 7) suggest that these clusters may be of interest for further theoretical and experimental investigations of chiroptical materials and optically active nanosystems. Figure 15 shows that the CD spectra of the Zr-adsorbed clusters differ in band number, sign pattern, and intensity. ZrB_7 (Fig. 15b) gives the strongest response, with a positive band at about 465 nm and a negative band at about 565 nm. ZrB_6 shows a positive band at about 380 nm and a negative band at about 460 nm. ZrB_8 shows several alternating bands between 320 and 470 nm. Zr_2B_6 and Zr_2B_7 (Figs. 15c and 15d) show weaker bands near 500 nm, one to two orders of magnitude below ZrB_7. These differences show that the chiroptical response depends on both the cluster geometry and the rotational strengths of its electronic transitions.

4 | Conclusion

A systematic theoretical investigation was performed on pristine B_n and Zr-adsorbed B_n (n = 6–8) clusters using density functional theory (DFT) with the B3LYP functional in combination with the

SDD and LanL2DZ basis sets. The optimized geometries, relative stabilities, structural and electronic properties, and reactivity characteristics of the investigated clusters were systematically analyzed using adsorption energy, ionization potential, electron affinity, and other relevant descriptors. Among the investigated structures, the Zr_2B_8 cluster exhibits the highest overall stability based on the combined energetic and electronic analyses.

The vibrational frequency calculations confirm the stability of the optimized structures, except for pristine B_6, which exhibits an imaginary vibrational frequency. The HOMO–LUMO analysis demonstrates that Zr adsorption significantly modifies the electronic structure of the boron clusters. The variation in the HOMO–LUMO energy gaps between pyramidal and bipyramidal configurations indicates differences in their relative chemical stability and reactivity. The global reactivity descriptors further show that Zr adsorption generally increases the chemical hardness and decreases the softness and electrophilicity of the clusters, indicating a tendency toward lower chemical reactivity. Among the investigated systems, Zr_2B_8 exhibits the highest chemical hardness, consistent with its comparatively stable electronic structure.

The ionization potentials and electron affinities, estimated within the Koopmans approximation, indicate that Zr adsorption changes the electron-donating and electron-accepting character of the boron clusters. The DOS analysis shows a corresponding redistribution of the electronic states, and the spin-resolved DOS of Zr_2B_7 shows pronounced spin polarization, which may merit further study for spin-dependent applications. The absorption spectra show hypsochromic shifts for the B_6- and B_7-based systems and a bathochromic shift for the B_8-based system, and the CD spectra show distinct chiroptical responses for selected Zr-containing clusters. These results indicate that Zr adsorption can tune the structural, electronic, optical, and spin-related properties of small boron clusters.

Overall, the present results show that Zr adsorption modifies the stability, chemical reactivity, spin polarization, and optical response of B_n (n = 6–8) clusters. These findings provide a basis for further theoretical and experimental studies. Future work may examine the emission and reflection spectra, catalytic activity, and interaction with reactive gas molecules of these clusters, to assess their potential in optoelectronic, sensing, catalytic, and spin-dependent applications.

Reference

1. Yao, J. G., Wang, X. W., and Wang, Y. X., (2008). A theoretical study on structural and electronic properties of Zr-doped B clusters: ZrB_n (n = 1-12). Chem Phys, 351(1-3): 1–6.

2. Ma, J., Li, Z., Fan, K., and Zhou, M., (2003). Density functional theory study of the B_6, B_6^+, B_6^-, and B_6^{2-} clusters. Chem Phys Lett., 372(5-6): 708–716.

3. Lau, K. C., Deshpande, M., Pati, R., and Pandey, R., (2005). A theoretical study of electronic and vibrational properties of neutral, cationic, and anionic B_{24} clusters. Int J Quantum Chem., 103(6):866–874.

4. Yadav, M. K., Sanyal, B., and Mookerjee, A., (2009). Structural, electronic and magnetic properties of Cr-doped $(ZnTe)_{12}$ clusters. J Magn Magn Mater., 321(4):235–240.

5. Tai, T. B., and Nguyen, M. T., (2010). Thermochemical properties, electronic structure and bonding of mixed lithium boron clusters (B_nLi, n = 1-8) and their anions. Chem Phys., 375(1):35–45.

6. Yang, Z., and Xiong, S. J., (2008). Structures and electronic properties of small FeB_n (n = 1-10) clusters. J Chem Phys., 128(18):184310.

7. Feng, X. J., and Luo, Y. H., (2007). Structure and stability of Al-doped boron clusters by the density-functional theory. J Phys Chem A., 111(12):2420–2425.

8. Li, W. L., Chen, Q., Tian, W. J., Bai, H., Zhao, Y. F., Hu, H. S., Li, J., Zhai, H. J., Li, S. D., and Wang, L. S., (2014). The B_{35} cluster with a double-hexagonal vacancy: a new and more flexible structural motif for borophene. J Am Chem Soc., 136(35):12257–12260.

9. Boustani, I., (1995). Structure and stability of small boron clusters: a density functional theoretical study. Chem Phys Lett., 240(1-3):135–140.

10. Alexandrova, A. N., Boldyrev, A. I., Zhai, H. J., Wang, L. S., Steiner, E., and Fowler, P. W., (2003). Structure and bonding in B_6^- and B_6: planarity and antiaromaticity. J Phys Chem A., 107(9):1359–1369.

11. Zhai, H. J., Wang, L. S., Alexandrova, A. N., Boldyrev, A. I., and Zakrzewski, V. G., (2003). Photoelectron spectroscopy and ab initio study of B_3^- and B_4^- anions and their neutrals. J Phys Chem A., 107(44):9319–9328.

12. Zhai, H. J., Wang, L. S., Alexandrova, A. N., and Boldyrev, A. I., (2002). Electronic structure and chemical bonding of B_5^- and B_5 by photoelectron spectroscopy and ab initio calculations. J Chem Phys., 117(17):7917–7924.

13. Li, Q. S., Gong, L. F., and Gao, Z. M., (2004). Structures and stabilities of B_7, B_7^+ and B_7^- clusters. Chem Phys Lett., 390(1-3):220–227.

14. Li, Q. S., and Jin, H. W., (2002). Structure and stability of B_5, B_5^+, and B_5^- clusters. J Phys Chem A., 106(30):7042–7047.

15. Li, Q., Zhao, Y., Xu, W., and Li, N., (2005). Structure and stabil-

ity of B_8 clusters. Int J Quantum Chem., 101(2):219–229.

16. Zhang, L. N., Jia, J., and Wu, H. S., (2015). Structural and electronic properties of V_2B_n (n = 1–10) clusters. Chem Phys., 459:131–136.

17. Romanescu, C., Galeev, T. R., Li, W. L., Boldyrev, A. I., and Wang, L. S., (2013). Transition-metal-centered monocyclic boron wheel clusters (M©B_n): a new class of aromatic borometallic compounds. Acc Chem Res., 46(2):350–358.

18. Liu, X., Zhao, G. F., Guo, L. J., Jing, Q., and Luo, Y. H., (2007). Structural, electronic, and magnetic properties of MB_n (M = Cr, Mn, Fe, Co, Ni; n ≤ 7) clusters. Phys Rev A., 75(6):063201.

19. Chen, Z. Q., Peng, Y. S., Hu, M., Li, C. M., and Luo, Y. T., (2016) Elasticity, hardness, and thermal properties of ZrB_n (n = 1, 2, 12). Ceram Int., 42(6):6624–6631.

20. Jia, J., Ma, L., Wang, J. F., and Wu, H. S., (2013). Structures and stabilities of ScB_n (n = 1-12) clusters: an ab initio investigation. J Mol Model., 19(8):3255–3261.

21. Barysz, M., and Urban, M., (1997). Molecular properties of boron-coinage metal dimers: BCu, BAg, BAu. Adv Quantum Chem., 28:257–272.

22. Zhai, H. J., Wang, L. S., Zubarev, D. Y., and Boldyrev, A. I., (2006). Gold apes hydrogen: the structure and bonding in the planar B_7Au_2- and B_7Au_2 clusters. J Phys Chem A., 110(5):1689–1693.

23. Li, W. L., Xie, L., Jian, T., Romanescu, C., Huang, X., and Wang, L. S., (2014). Hexagonal bipyramidal $[Ta_2B_6]^-/0$ clusters: B_6 rings as structural motifs. Angew Chem Int Ed., 53(5):1288–1292.

24. Fokwa, B. P. T., and Hermus, M., (2012). All-boron planar B_6 ring in the solid-state phase $Ti_7Rh_4Ir_2B_8$. Angew Chem Int Ed., 51(7):1702–1705.

25. Jia, J., Li, X., Li, Y., Ma, L., and Wu, H. S., (2014). Density functional theory investigation on the structure and stability of Sc_2B_n (n = 1–10) clusters. Comput Theor Chem., 1027:128–134.

26. Zhang, Z., Penev, E. S., and Yakobson, B, I., (2017). Two-dimensional boron: structures, properties and applications. Chem Soc Rev., 46(22):6746–6763.

27. Mannix, A. J., Zhou, X. F., Kiraly, B., Wood, J. D., Alducin, D., Myers, B. D., Liu, X., Fisher, B. L., Santiago, U., Guest, J. R., Yacaman, M. J., Ponce, A., Oganov, A. R., Hersam, M. C., and Guisinger, N. P., (2015). Synthesis of borophenes: anisotropic, two-dimensional boron polymorphs. Science., 350(6267):1513–1516.

28. Tai, G., Hu, T., Zhou, Y., Wang, X., Kong, J., Zeng, T., You, Y., and Wang, Q., (2015). Synthesis of atomically thin boron films on copper foils. Angew Chem Int Ed., 54(51):15473–15477.

29. Frisch, M. J., Trucks, G. W., Schlegel, H. B., Scuseria, G. E., Robb, M. A., Cheeseman, J. R., et al., (2016). Gaussian 16, Revision B.01. Wallingford, CT: Gaussian, Inc.; 2016.

30. Lee, C., Yang, W., and Parr, R. G., (1988). Development of the Colle-Salvetti correlation-energy formula into a functional of the electron density. Phys Rev B., 37(2):785–789.

31. Fuentealba, P., Stoll, H., Von, Szentpaly, L., Schwerdtfeger, P., and Preuss, H., (1983). On the reliability of semi-empirical pseudopotentials: simulation of Hartree-Fock and Dirac-Fock results. J Phys B At Mol Phys., 16(11): L323-L328.

32. Fabiano, E., Sala, F. D., and Cingolani, R., (2004). Ab-initio study of singlet and triplet excitation energies in oligothiophenes. Phys Status Solidi C., 1(3):539–542.

33. Hay, P. J., and Wadt, W. R., (1985). Ab initio effective core potentials for molecular calculations: potentials for K to Au including the outermost core orbitals. J Chem Phys., 82(1):299–310.

34. Cao, X., and Dolg, M., (2004). Segmented contraction scheme for small-core actinide pseudopotential basis sets. J Mol Struct THEOCHEM,. 673(1-3):203–209.

35. Zou, M., Zhang, J., Chen, J., and Li, X., (2012). Simulating adsorption of organic pollutants on finite (8,0) single-walled carbon nanotubes in water. Environ Sci Technol, 46(16):8887–8894.

36. Rad, A. S., Shabestari, S. S., Jafari, S. A., Zardoost, M. R., and Mirabi, A., (2016). N-doped graphene as a nanostructure adsorbent for carbon monoxide: DFT calculations. Mol Phys., 114(11):1756–1762.

37. Rad, A. S., (2015). First principles study of Al-doped graphene as nanostructure adsorbent for NO_2 and N_2O: DFT calculations. Appl Surf Sci., 357(A):1217–1224.

38. Pérez, P., Toro-Labbé, A., and Contreras, R., (2001). Solvent effects on electrophilicity. J Am Chem Soc., 123(23):5527–5531.

39. Rezaei-Sameti, M., (2012). The effect of doping three Al and N atoms on the chemical shielding tensor parameters of the boron phosphide nanotubes: a DFT study. Phys B Condens Matter, 407(1):22–26.

40. Rezaei-Sameti, M., and Yaghoobi, S., (2015). Theoretical study of adsorption of CO gas on pristine and AsGa-doped (4,4) armchair models of BPNTs. Comput Condens Matter, 3:21–29.

41. Hay, P. J., and Wadt, W. R., (1985). Ab initio effective core potentials for molecular calculations: potentials for main group elements Na to Bi. J Chem Phys., 82(1):284–298.

42. Kato, H., and Tanaka, E., (1991). Stabilities of small Ben and B_n clusters (4 ≤ n ≤ 8) by vibrational analysis. J Comput Chem., 12(9):1097–1109.

43. Mulliken, R. S., (1955). Electronic population analysis on LCAO-MO molecular wave functions. II. Overlap populations, bond orders, and covalent bond energies. J Chem Phys., 23(10):1841–1846.

44. Bulat, F. A, Burgess, J. S., Matis, B. R., Baldwin, J. W., Macaveiu, L., Murray, J. S., and Politzer, P., (2012). Hydrogenation and fluorination of graphene models: analysis via the average local ionization energy. J Phys Chem A., 116(33):8644–8652.

45. Bulat, F. A., Toro-Labbé, A., Brinck, T., Murray, J. S., and Politzer, P., (2010). Quantitative analysis of molecular surfaces: areas, volumes, electrostatic potentials and average local ionization energies. J Mol Model, 16(11):1679–1691.

46. Murray, J. S., and Politzer, P., (2011). The electrostatic potential: an overview. WIREs Comput Mol Sci., 1(2):153–163.

47. Zhan, C. G., Nichols, J. A., and Dixon, D. A., (2003). Ionization potential, electron affinity, electronegativity, hardness, and electron excitation energy: molecular properties from density functional theory orbital energies. J Phys Chem A., 107(20):4184–4195.

48. Rad, A. S., Valipour, P., Gholizade, A., and Mousavinezhad, S. E., (2015). Interaction of SO_2 and SO_3 on terthiophene (as a model of polythiophene gas sensor): DFT calculations. Chem Phys Lett., 639:29–35.

49. Pearson, R. G., (2005). Chemical hardness and density functional theory. J Chem Sci., 117(5):369–377.

50. Zhou, Z., and Parr, R. G., (1990). Activation hardness: new index for describing the orientation of electrophilic aromatic substitution. J Am Chem Soc., 112(15):5720–5724.

51. Xu, S., Dong, R., Lv, C., Wang, C., and Cui, Y., (2017). Configurations and characteristics of boron and B_{36} clusters. J Mol Model, 23(7):198.

52. Job, G., and Herrmann, F., (2006). Chemical potential—a quantity in search of recognition. Eur J Phys., 27(2):353–371.

53. Hu, X., (2012). Half-metallic antiferromagnet as a prospective material for spintronics. Adv Mater, 24(2):294–298.

54. Yadav, P. S., Pandey, D. K., Agrawal, S., and Agrawal, B. K., (2010). Ab initio study of structural, electronic, optical, and vibrational properties of Zn_xS_y (x + y = 2 to 5) nanoclusters. J Nanopart Res., 12(3):737–757.

55. Adler, A. J., Greenfield, N. J., and Fasman, G. D., (1973). Circular dichroism and optical rotatory dispersion of proteins and polypeptides. Methods Enzymol. 27:675–735.

56. Pecul, M., and Ruud, K., (2005). The ab initio calculation of optical rotation and electronic circular dichroism. Adv Quantum Chem., 50:185–212.

Acknowledgements
The authors extend sincere gratitude to the authority of the Bangladesh Atomic Energy Regulatory Authority, Dhaka, Bangladesh.

Funding
The authors declare that no funds, grants, or other support were received during the preparation of this manuscript. The investigation was not funded by any organization or any sources.

Ethics Statement
The submitted work is a unique contribution to the field, not published elsewhere in any form or language. Results are presented clearly, honestly, and without fabrication, falsification or inappropriate data manipulation. Authors adhere to discipline-specific rules for acquiring, selecting and processing data.

Conflicts of Interest
The authors declare no conflicts of interest.

Authors Contribution
All authors contributed to the study conception, validation and review-editing. Investigation, methodology, Material preparation, data curation, formal analysis, writing – original draft, visualization, software were performed by Mosa Farzana Israt and Md. Kabir Ahamed. The first draft of the manuscript was written by Mosa Farzana Israt and all authors commented on previous versions of the manuscript. All authors read and approved the final manuscript.

Data Availability Statement
The data that support the findings of this study are available on request from the corresponding author.